AIAA JOURNAL
Vol. 49, No. 3, March 2011

System Identification for Coupled Fluid–Structures: Aerodynamics is Aeroelasticity Minus Structure

Taehyoun Kim*
The Boeing Company, Seattle, Washington 98124-2207

DOI: 10.2514/1.J050245

A new method that identifies coupled fluid–structure systems with a reduced set of state variables is presented. Assuming that the structural model is known a priori, from either an analysis or a test and using linear transformations between structural and aeroelastic states, it is possible to deduce aerodynamic information from sampled time histories of the aeroelastic system. More specifically, given a finite set of structural modes, the method extracts a generalized aerodynamic force matrix corresponding to these mode shapes. Once the aerodynamic forces are known, an aeroelastic reduced-order model can be constructed in discrete-time state-space format by coupling the structural model and the aerodynamic system. It is demonstrated that the resulting reduced-order models are accurate, robust, and suitable for aeroelastic analysis at constant Mach, varying density conditions.

Nomenclature

$\mathbf{A}$, $\mathbf{B}$, $\mathbf{C}$	=	structural system matrices
$\mathbf{A}_a$, $\mathbf{B}_a$, $\mathbf{C}_a$, $\mathbf{D}_a$	=	aerodynamic system matrices
$\mathbf{A}_t$, $\mathbf{B}_t$, $\mathbf{C}_t$	=	aeroelastic system matrices
$\mathbf{A}_{ta}$	=	aerodynamic submatrix defined in Eq. (28)
$\mathbf{C}_{ta}$	=	aerodynamic output submatrix defined in Eq. (33)
$\mathbf{F}$	=	forcing input matrix for structure
$\mathbf{G}$	=	generalized damping matrix
$\mathbf{K}$	=	generalized stiffness matrix
$\mathbf{M}$	=	generalized mass matrix
M	=	number of time steps
Mach	=	Mach number
N	=	number of structural modes or displacement measurements
na	=	number of aerodynamic measurements
$\mathbf{p}$	=	$(N \times 1)$ generalized coordinates vector
q	=	$\frac{1}{2}\rho V^2$
Q_{ij}	=	generalized aerodynamic force coefficients
q_{ref}	=	reference dynamic pressure at which aeroelastic responses are sampled
R	=	dimension of structural states vector $\mathbf{x}$
Re	=	Reynolds number
R_t	=	dimension of aeroelastic states vector $\mathbf{Y}$
t	=	real time
$\mathbf{T}_\zeta$	=	transformation matrix from $\mathbf{Y}$ to $\mathbf{x}$
$\mathbf{T}_\eta$	=	transformation matrix from $\mathbf{x}$ to $\mathbf{Y}_x$
$\mathbf{U}$, $\mathbf{\Sigma}$, $\mathbf{V}$	=	singular value decomposition matrices
$\mathbf{u}$	=	control inputs vector
V	=	freestream airspeed
$\mathbf{v}$	=	(na $\times$ 1) aerodynamic measurements' vector
V_{ref}	=	reference airspeed at which aeroelastic responses are sampled
$\mathbf{w}$	=	$\begin{Bmatrix} \mathbf{z} \\ \dot{\mathbf{z}} \end{Bmatrix}$
$\mathbf{x}$	=	$(R \times 1)$ structural states vector
$\mathbf{Y}$	=	$(R_t \times 1)$ aeroelastic states vector
$\mathbf{y}$	=	aerodynamic states vector
$\mathbf{Y}_x$	=	$(R_t \times 1)$ structural substates vector
$\mathbf{Y}_y$	=	$(R_t \times 1)$ aerodynamic substates vector
$\mathbf{z}$	=	$(N \times 1)$ displacement measurements' vector
ρ	=	air density
$\mathbf{\Phi}$	=	structural sensor matrix

Received 24 September 2009; revision received 25 October 2010; accepted for publication 26 October 2010.

*taehyoun.kim@boeing.com. Associate Fellow AIAA.

Introduction

In THE last decade, much research has been conducted on model reduction and system identification of coupled fluid–structure systems. It first started with the eigenanalysis of fluid dynamic systems in which, similar to the concept of natural frequencies and mode shapes in structural dynamics, eigenvalues and eigenvectors of the flowfield are identified and used to construct a reduced-order model (ROM) of the unsteady aerodynamic system [1,2]. Although it was a novel idea, calculating the aerodynamic eigenmodes is costly due to the nonsymmetric and nonconservative nature of the fluid dynamic systems. Later, the eigenmodes were replaced by the proper orthogonal decomposition (also known as the Karhunen–Loeve procedure) modes, making the modal analysis more feasible and practical, as it is relatively straightforward to calculate the optimal modes based on actual time or frequency samples [3–6]. However, to apply the modal analysis, it is necessary to have the original system equations available. Normally, only a small amplitude oscillation around a static solution is sought in this type of analysis, so the system equations should be obtained by perturbing the original nonlinear equations about the static equilibrium point. Unfortunately, most of the available computational fluid dynamic (CFD) codes do not have dynamically linearized operators, nor do they allow easy access to the system equations. To remedy this, system identification methods have been used toward model reduction of aerodynamic systems [7–11]. Unlike the modal analysis, the system identification is essentially a black box approach in which only system inputs and outputs are considered and, as such, there is a potential danger of losing detailed information about the underlying aerodynamics. More important, as Schuster et al. [12] pointed out, when the number of structural modes increases, the CPU time to get all of the corresponding aerodynamic forces increases proportionally, surpassing the CPU time that is required for a typical static CFD run. This downside, which is also true of the modal methods, was overcome by Kim and Bussoletti [6], Kim et al. [10], and Kim [13] by the so-called single-composite-input (SCI) approach. The idea is that, if the system is linear and has multiple driving inputs (e.g., an unsteady CFD code subjected to multiple structural mode inputs), one can excite the multiple input channels simultaneously with statistically independent signals instead of exciting the flowfield with one mode shape at a time. The simultaneous excitation of multiple mode shapes was also explored by Silva, using a series of orthogonal time functions [14]. Apart from the multiple structural modes, it is often necessary to check the aircraft performance for a variety of

flight conditions that involve multiple Mach numbers, payloads, and fuel conditions, among others. Recently, an interpolation scheme based on the Grassman manifold has been shown to be efficient in reducing the model construction time for the multiple flight conditions [15].

In all of the aforementioned methods, the aerodynamic systems are treated separately from the structural systems. From the structural engineers' perspective, this makes the procedure of model reduction cumbersome and challenging, in that they need to have either detailed knowledge of the CFD code or extensive help from well-trained CFD engineers. Furthermore, there is little chance of using data from a wind-tunnel test (WTT) or a flight flutter test (FFT), because the data are normally obtained from the coupled aeroelastic system rather than the isolated aerodynamic system. Nissim and Gilyard [16] developed a frequency domain identification scheme in which the aerodynamic as well as the structural system matrices are extracted by manipulating frequency responses from the airplane at two different dynamic pressures. Its main limitation is that a quasi-steady approximation is required in the unsteady aerodynamics to minimize the number of unknowns and make the matrix operations robust and solvable.

In this paper, a novel system identification and model reduction technique for linear time-invariant coupled fluid–structure systems is introduced. Unlike all of the existing methods discussed previously, the new method works directly on time history data of the coupled aeroelastic system measured at a single flight condition. Assuming that structural properties are known a priori and using linear transformations between structural and aeroelastic states, it is possible to reconstruct the aerodynamic system given a finite set of structural modes. Once the aerodynamic model is obtained, an aeroelastic ROM can be constructed in discrete-time state-space format by coupling the structural model and the aerodynamic system.

For demonstration, the proposed method is applied to two different lifting surface configurations interacting with two different flowfields. One is subsonic incompressible flow modeled by the vortex lattice method (VLM), and the other is viscous transonic aerodynamic flow modeled by the CFL3D code. The structural configurations used in this investigation are a flat rectangular wing and a scaled commercial airplane wind-tunnel model. Impulse responses of both the airplane motion and aerodynamic quantities are sampled and processed at a subcritical condition. The aerodynamic system is then identified by subtracting the structural substates from the aeroelastic states. It is shown that, when sufficient aerodynamic measurements are available, the identified generalized aerodynamic force (GAF) elements match extremely well with the original values for all the frequencies of interest. As a result, the aeroelastic ROM can predict aeroelastic responses at any dynamic pressure very accurately, making the constant Mach, varying density (CMVD) analysis possible. It is also shown that, even when only a few or no aerodynamic samples are available, the method still predicts the onset of the flutter fairly well, provided that the structural motion was observed at a speed not far from the flutter speed. This is promising, especially for the purpose of aeroelastic damping and flutter prediction based on WTT or FFT, as it is often expensive and difficult to measure unsteady pressures during the tests.

Basic Assumptions

We will assume that time histories of airplane structural and aerodynamic responses due to certain inputs (e.g., control surfaces) are available at both zero and nonzero airspeeds. The structural responses here are displacements and velocities at various locations on the airplane, whereas the aerodynamic responses could be pressure data (especially in the case of tests) or, in the case of numerical simulations, any of the independent aerodynamic variables, such as vortices and potentials in the flowfield.

The following assumptions are also made:

1) Structure, aerodynamics, and aeroelasticity are all dynamically linear, i.e., have small perturbed oscillations.

2) The airplane is flying along a CMVD curve.

3) A sufficient number of the structural and aeroelastic measurements are available.

4) Background noise in the data is minimal or has been subdued by standard signal processing.

5) The system is controllable and observable.

Structural and Aerodynamic Measurements

First, airplane responses are taken at M time steps ($t = 0,\ \Delta t,\ 2\Delta t, \ldots, (M-1)\Delta t$) on the ground and in the air, respectively:

$$[\,\mathbf{w}^0 \quad \mathbf{w}^1 \quad \mathbf{w}^2 \quad \ldots \quad \mathbf{w}^{M-1}\,], \qquad V = 0 \tag{1}$$

$$\begin{bmatrix} \mathbf{v}^0 & \mathbf{v}^1 & \mathbf{v}^2 & \ldots & \mathbf{v}^{M-1} \\ \mathbf{w}^0 & \mathbf{w}^1 & \mathbf{w}^2 & \ldots & \mathbf{w}^{M-1} \end{bmatrix}, \qquad V = V_{\text{ref}} \tag{2}$$

These time samples represent the structural dynamic and aeroelastic systems, respectively, and could be obtained from either computational structural dynamics (CSD)/CFD simulations or from a ground vibration test (GVT)/WTT or FFT (see Fig. 1).

Once we have collected the time history samples, we can identify the system output matrices using standard data processing. For instance, singular value decomposition (SVD) produces

$$[\,\mathbf{w}^0 \quad \mathbf{w}^1 \quad \mathbf{w}^2 \quad \ldots \quad \mathbf{w}^{M-1}\,]_{V=0} \simeq \mathbf{U}_R \boldsymbol{\Sigma}_R^{1/2} \cdot \boldsymbol{\Sigma}_R^{1/2} \mathbf{V}_R^T \equiv \mathbf{C}[\,\mathbf{x}^0 \quad \mathbf{x}^1 \quad \mathbf{x}^2 \quad \ldots \quad \mathbf{x}^{M-1}\,] \tag{3}$$

$$\begin{bmatrix} \mathbf{v}^0 & \mathbf{v}^1 & \mathbf{v}^2 & \ldots & \mathbf{v}^{M-1} \\ \mathbf{w}^0 & \mathbf{w}^1 & \mathbf{w}^2 & \ldots & \mathbf{w}^{M-1} \end{bmatrix}_{V=V_{\text{ref}}} \simeq \mathbf{U}_{R_t} \boldsymbol{\Sigma}_{R_t}^{1/2} \cdot \boldsymbol{\Sigma}_{R_t}^{1/2} \mathbf{V}_{R_t}^T \equiv \mathbf{C}_t[\,\mathbf{Y}^0 \quad \mathbf{Y}^1 \quad \mathbf{Y}^2 \quad \ldots \quad \mathbf{Y}^{M-1}\,] \tag{4}$$

where

$$\mathbf{C}_t \equiv \begin{bmatrix} \mathbf{C}_v \\ \mathbf{C}_w \end{bmatrix} \tag{5}$$

Note that the realization by SVD guarantees the matrices with minimum sizes. That is, R and R_t are the ranks of the data covariance matrices associated with the structural and aeroelastic time samples.

Topology and Transformation of States

Within the aeroelastic system, one can split the aeroelastic states $\mathbf{Y}$ into the structural part $\mathbf{Y}_x$ and the aerodynamic part $\mathbf{Y}_y$. The dimension of the substate vectors is R_t, but they are rank deficient (i.e., have ranks smaller than R_t) (see Fig. 2 for topological description).

Since both the structural and aeroelastic samples contain the common structural set $\mathbf{w}$, it is possible to relate between $\mathbf{x}$, $\mathbf{Y}$, and $\mathbf{Y}_x$ through transformation matrices. Toward this end, we will assume that, during the flight, the structure behaves the same way as described by CSD or GVT. That is, the output matrix $\mathbf{C}$, relating the structural states and the responses, still satisfies Eq. (3), except that $\mathbf{x}$ now represents the structural states within the aeroelastic system. Equating Eq. (3) and the structural portion of Eq. (4) yields

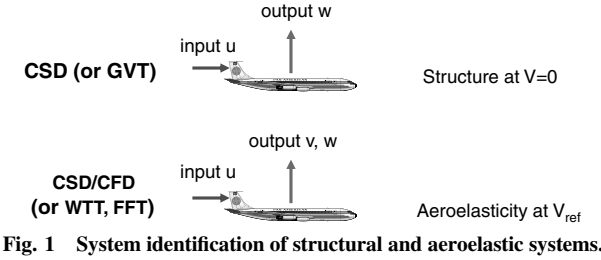

Fig. 1 System identification of structural and aeroelastic systems.

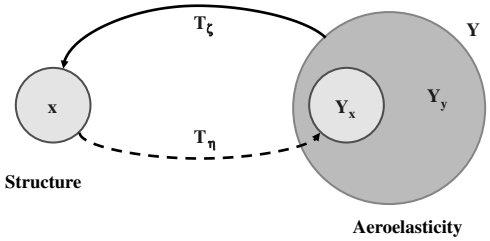

Fig. 2 Topology and transformation of states.

$$\mathbf{x} = \mathbf{T}_\zeta \mathbf{Y} \tag{6}$$

$$\mathbf{Y}_x = \mathbf{T}_\eta \mathbf{x} \tag{7}$$

where

$$\mathbf{T}_\eta \equiv \mathbf{C}_{t2}^{-p}\mathbf{C} \tag{8}$$

$$\mathbf{T}_\zeta \equiv \mathbf{C}^{-p}\mathbf{C}_w \tag{9}$$

$$\mathbf{I} \equiv \mathbf{T}_\zeta \mathbf{T}_\eta \tag{10}$$

and

$$\mathbf{C}_{t2}^{-p} \equiv \text{last 2N columns of } \mathbf{C}_t^{-p} \tag{11}$$

Here, $(\,)^{-p}$ denotes pseudoinversion of the matrix.

Relation Between x, Y, and Y_x

Since $\mathbf{v}$ and $\mathbf{w}$ each contain only the aerodynamic and structural response, respectively, $\mathbf{Y}_x$ and $\mathbf{Y}_y$ are additive and complementary, satisfying the following property:

$$\mathbf{Y} = \mathbf{Y}_x + \mathbf{Y}_y = \mathbf{f}_x(\mathbf{Y}) + \mathbf{f}_y(\mathbf{Y}) \tag{12}$$

where $\mathbf{f}_x$ and $\mathbf{f}_y$ represent mappings from the aeroelastic states to the structural and aerodynamic substates:

$$\mathbf{f}_x \equiv \mathbf{T}_\eta \mathbf{T}_\zeta \tag{13}$$

$$\mathbf{f}_y \equiv \mathbf{I} - \mathbf{T}_\eta \mathbf{T}_\zeta \tag{14}$$

Additional Properties of f_x and f_y

It can be shown that $\mathbf{f}_x$ and $\mathbf{f}_y$ themselves are also complementary and hence satisfy

$$\mathbf{f}_x(\mathbf{f}_y) = \mathbf{0} \tag{15}$$

$$\mathbf{f}_y(\mathbf{f}_x) = \mathbf{0} \tag{16}$$

Said another way, structural mapping on aerodynamics and aerodynamic mapping on structure produce zeros.

Also,

$$\mathbf{f}_x(\mathbf{f}_x) = \mathbf{f}_x \tag{17}$$

$$\mathbf{f}_y(\mathbf{f}_y) = \mathbf{f}_y \tag{18}$$

That is, structural mapping on structure and aerodynamic mapping on aerodynamics produce themselves.

Structural and Aeroelastic Systems in Time Domain

Along with the identification of the output matrices and states, full realizations of the structural and aeroelastic systems can be obtained in discrete-time state-space format using standard system identification methods such as the Eigensystem Realization Algorithm (ERA) [17], the autoregressive moving average [18], the observer/Kalman filter identification (OKID) [17], and the SCI/ERA [13].

Structure:

$$\mathbf{x}^{n+1} = \mathbf{A}\mathbf{x}^n + \mathbf{B}\mathbf{u}^n \tag{19}$$

$$\mathbf{w}^n = \mathbf{C}\mathbf{x}^n \tag{20}$$

Aeroelasticity:

$$\mathbf{Y}^{n+1} = \mathbf{A}_t \mathbf{Y}^n + \mathbf{B}_t \mathbf{u}^n \tag{21}$$

$$\begin{Bmatrix} \mathbf{v}^n \\ \mathbf{w}^n \end{Bmatrix} = \mathbf{C}_t \mathbf{Y}^n = \begin{bmatrix} \mathbf{C}_v \\ \mathbf{C}_w \end{bmatrix} \mathbf{Y}^n \tag{22}$$

Alternatively, the structural model could also be obtained from a finite element method expressing the structural equations of motion in terms of a finite number of mode shapes. If desired, the computational model can be updated based on the GVT data. In this case, the structural mass, damping, stiffness, and forcing matrices will be available to construct an equation of motion in continuous time:

$$\mathbf{M}\ddot{\mathbf{p}} + \mathbf{G}\dot{\mathbf{p}} + \mathbf{K}\mathbf{p} = \mathbf{F}\mathbf{u} \tag{23}$$

from which Eqs. (19) and (20) are obtained by discretizing the time derivatives with the incremental time step Δt. Note that the structural states are the modal displacements and modal velocities; that is, $\mathbf{x} \equiv \lfloor \mathbf{p}\dot{\mathbf{p}} \rfloor^T$ and

$$\mathbf{z} = \mathbf{\Phi}\mathbf{p} \tag{24}$$

where $\mathbf{\Phi}$ is a sensor matrix that transforms the modal coordinates to the physical displacements.

Identification of Aerodynamic System

Differential equations for the aerodynamics can be found by subtracting the structural substates from the aeroelastic states:

$$\mathbf{Y}_y^{n+1} = \mathbf{Y}^{n+1} - \mathbf{Y}_x^{n+1} \tag{25}$$

which, after using Eqs. (7) and (21), becomes

$$\mathbf{Y}_y^{n+1} = \mathbf{A}_t(\mathbf{Y}_y^n + \mathbf{T}_\eta \mathbf{x}^n) + \mathbf{B}_t \mathbf{u}^n - \mathbf{T}_\eta \mathbf{x}^{n+1} \tag{26}$$

Transforming both sides by $\mathbf{f}_y$ yields, after using the properties in Eqs. (16) and (18),

$$\mathbf{Y}_y^{n+1} = \mathbf{A}_{ta}\mathbf{Y}_y^n + \mathbf{A}_{ta}\mathbf{T}_\eta \mathbf{x}^n \tag{27}$$

where

$$\mathbf{A}_{ta} \equiv (\mathbf{I} - \mathbf{T}_\eta \mathbf{T}_\zeta)\mathbf{A}_t \tag{28}$$

Equation (27) is a system realization of the underlying unsteady aerodynamics. Note carefully that the aerodynamic substates $\mathbf{Y}_y$ are driven by the structural states $\mathbf{x}$: the only source of driving input for the unsteady flowfield in the absence of external disturbances, such as gust. Note that $\mathbf{A}_{ta}$ is singular, because the transformation $\mathbf{I} - \mathbf{T}_\eta \mathbf{T}_\zeta$ is a singular matrix. Using Eqs. (7) and (12), Eq. (27) can be rewritten in a more compact form:

$$\mathbf{Y}_y^{n+1} = \mathbf{A}_{ta}\mathbf{Y}^n \tag{29}$$

It simply states that the aerodynamic submatrix transforms the aeroelastic states at the current time step into the aerodynamic substates at the next time step.

The corresponding aerodynamic force is found by subtracting the input force from the sum of the inertia, damping, and elastic forces according to the D'Alembert's principle:

$$\mathbf{F}^n = \mathbf{x}^{n+1} - \mathbf{A}\mathbf{x}^n - \mathbf{B}\mathbf{u}^n \tag{30}$$

$$= \mathbf{T}_\zeta \mathbf{A}_t \mathbf{Y}_y^n + (\mathbf{T}_\zeta \mathbf{A}_t \mathbf{T}_\eta - \mathbf{A})\mathbf{x}^n \tag{31}$$

$$\equiv \mathbf{C}_{ta}\mathbf{Y}^n - \mathbf{A}\mathbf{x}^n \tag{32}$$

with the aerodynamic output submatrix $\mathbf{C}_{ta}$ defined as

$$\mathbf{C}_{ta} \equiv \mathbf{T}_\zeta \mathbf{A}_t \tag{33}$$

It can be shown that the aeroelastic system matrix is related to $\mathbf{A}_{ta}$ and $\mathbf{C}_{ta}$ as

$$\mathbf{A}_t = \mathbf{A}_{ta} + \mathbf{T}_\eta \mathbf{C}_{ta} \tag{34}$$

$\mathbf{F}$ is given in terms of the mathematical states $\mathbf{x}$ that define the structural model. It is desirable to convert $\mathbf{x}$ to the physical coordinates $\mathbf{w}$ using Eq. (20). In this case, the identified aerodynamics can be easily put into the state-space form by a standard system identification method, using $\mathbf{z}$ as the only driving input to the flowfield:

$$\mathbf{y}^{n+1} = \mathbf{A}_a \mathbf{y}^n + \mathbf{B}_a \mathbf{z}^n \tag{35}$$

$$\mathbf{F}^n = q(\mathbf{C}_a \mathbf{y}^n + \mathbf{D}_a \mathbf{z}^n) \tag{36}$$

where $\mathbf{y}$ are the new aerodynamic states and $q \equiv \frac{1}{2}\rho V^2$ is the dynamic pressure. If $\mathbf{z}$ represents the modal coordinate vector $\mathbf{p}$, $\mathbf{F}$ becomes the GAF vector in the traditional sense.

Reduced-Order Aeroelastic Model

Coupled aeroelastic equations of motion can be obtained by coupling the identified aerodynamic system equations (27) and (32), with the structural dynamic equations (19) and (20). After rescaling Eq. (32) by the reference dynamic pressure, we obtain the following aeroelastic ROM:

$$\begin{Bmatrix} \mathbf{Y}_y^{n+1} \\ \mathbf{x}^{n+1} \end{Bmatrix} = \begin{bmatrix} \mathbf{A}_{ta} & \mathbf{A}_{ta}\mathbf{T}_\eta \\ q\mathbf{C}_{ta} & \mathbf{A} + q(\mathbf{C}_{ta}\mathbf{T}_\eta - \mathbf{A}) \end{bmatrix} \begin{Bmatrix} \mathbf{Y}_y^n \\ \mathbf{x}^n \end{Bmatrix} + \begin{bmatrix} \mathbf{0} \\ \mathbf{B} \end{bmatrix} \mathbf{u}^n \tag{37}$$

or, if we use Eqs. (35) and (36) instead,

$$\begin{Bmatrix} \mathbf{y}^{n+1} \\ \mathbf{w}^{n+1} \end{Bmatrix} = \begin{bmatrix} \mathbf{A}_a & [\mathbf{B}_a \quad \mathbf{0}] \\ q\mathbf{C}_a & \mathbf{A} + q[\mathbf{D}_a \quad \mathbf{0}] \end{bmatrix} \begin{Bmatrix} \mathbf{y}^n \\ \mathbf{w}^n \end{Bmatrix} + \begin{bmatrix} \mathbf{0} \\ \mathbf{B} \end{bmatrix} \mathbf{u}^n \tag{38}$$

It should be mentioned that Eq. (38) is valid for any combination of the air density and airspeed (ρ, V), making it possible to use the model for matched point solutions (i.e., at different altitudes with the Mach number fixed). In this case, one must allow the time step Δt to vary as a function of the airspeed according to $\Delta t = (V_{\text{ref}}/V)\Delta t_{\text{ref}}$. However, this is not feasible using Eq. (37), because the structural states vector $\mathbf{x}$ was defined for the reference time frame in which the time samples were taken. To remedy the drawback, the velocity coordinates are rescaled by V_{ref}/V, noting that the time derivatives should be adjusted to the new time scale:

$$\begin{Bmatrix} \mathbf{Y}_y^{n+1} \\ \mathbf{x}^{n+1} \end{Bmatrix} = \begin{bmatrix} \mathbf{A}_{ta} & [(\mathbf{A}_{ta}\mathbf{T}_\eta)_d \frac{V_{\text{ref}}}{V} (\mathbf{A}_{ta}\mathbf{T}_\eta)_v] \\ q\mathbf{C}_{ta} & \mathbf{A} + q[(\mathbf{C}_{ta}\mathbf{T}_\eta - \mathbf{A})_d \frac{V_{\text{ref}}}{V} (\mathbf{C}_{ta}\mathbf{T}_\eta - \mathbf{A})_v] \end{bmatrix} \times \begin{Bmatrix} \mathbf{Y}_y^n \\ \mathbf{x}^n \end{Bmatrix} + \begin{bmatrix} \mathbf{0} \\ \mathbf{B} \end{bmatrix} \mathbf{u}^n \tag{39}$$

where the subscripts d and v refer to the first and second halves of the structural coordinates corresponding to the displacements and velocities, respectively. With this modification, both aeroelastic systems in Eqs. (38) and (39) are valid for all dynamic pressure values at the fixed Mach number and, hence, can be used for CMVD analyses (e.g., flutter prediction, dynamic loads, and control system design). For example, taking a logarithm of the eigenvalues of the system matrix yields aeroelastic roots in the continuous-time domain and, hence, will determine the stability of the aeroelastic system.

Figure 3 represents an overall flowchart of the aeroelastic system identification process.

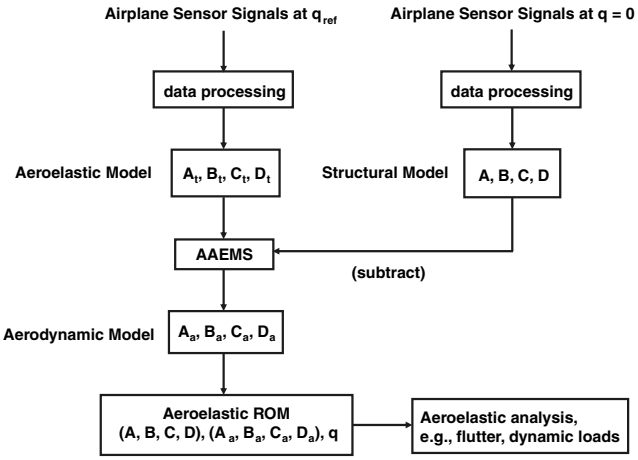

Fig. 3 Flowchart of aeroelastic system identification.

Results and Discussion

The proposed system identification scheme was applied to two different aeroelastic systems. They are a rectangular plate wing in a subsonic incompressible flow modeled by VLM and a transonic wind-tunnel model of a representative Boeing commercial airplane modeled by ELFINI and CFL3D.

It is reported that both types of aeroelastic ROMs, by Eqs. (38) and (39), were used, but they essentially yielded the same results. Therefore, all the results presented in the paper are based on the first ROM [Eq. (38)].

Rectangular Wing in Incompressible Flow

The first system is a rectangular flat wing with an aspect ratio of four (Fig. 4). The unsteady incompressible airflow is modeled by VLM, and the structural model is described by 12 coupled mode shapes. Since the structural model was already known from the basic analysis, the (12×12) generalized mass and stiffness matrices were directly used to construct (24×24) the structural system [Eqs. (19) and (20)]. To control the wing motion, four pairs of piezoelectric sensors/actuators are placed on the top and bottom sides of the wing. Input signals are applied to these actuators such that only a pure sectional moment is generated at each location. The unsteady flowfield is completely described by vortex ring elements on the free

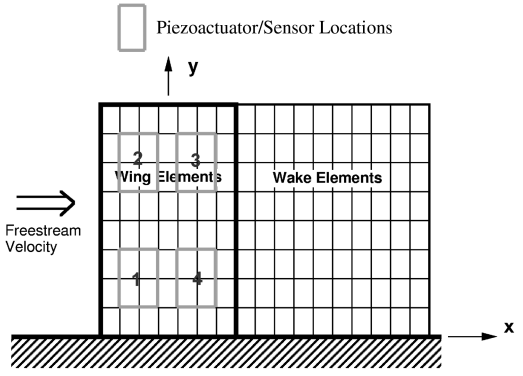

Fig. 4 Rectangular wing modeled by vortex lattice elements.

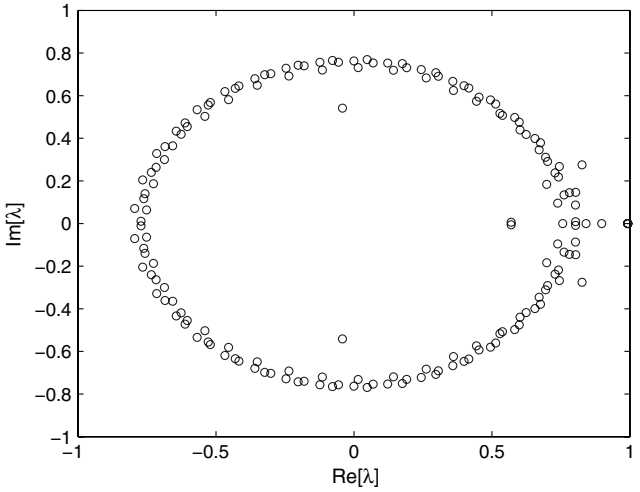

Fig. 5 Aerodynamic eigenvalues of VLM wing in the discrete-time domain.

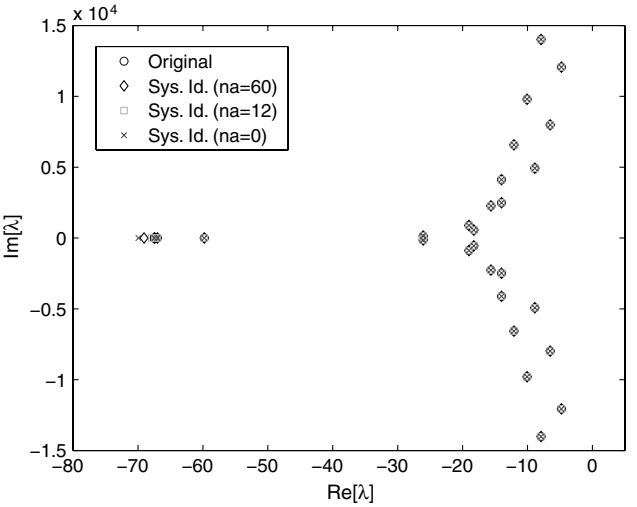

Fig. 6 Aeroelastic roots of VLM wing (circulatory part only) at $V_{\text{ref}} = 80$ m/s.

wake behind the wing. A total of 800 vortex rings were created on the wake, with 40 and 20 elements placed in the streamwise and spanwise directions. Thus, the size of the aeroelastic system is 824. For details of the model, see [13].[†]

To investigate the effect of aerodynamic measurement on the system realization, three different sets of sampled data were examined. They contain, in addition to the 24 structural samples (12 modal displacements plus 12 modal velocities), 0, 12, and 60 aerodynamic samples. The aerodynamic data here are arbitrary linear combinations of all of the 800 vortices. It should be mentioned that, being an incompressible flow model, the vortex lattice formulation includes both the noncirculatory and circulatory effects [19]. Since some of the noncirculatory terms are functions of accelerations of the structural motion, they are in the left-hand side of the aeroelastic equation of motion; hence, it is not possible to express them in the current format in Eq. (38) or Eq. (39), in which the unsteady aerodynamic loads are assumed to be proportional to the dynamic pressure. However, such a limitation will disappear once the flow becomes compressible, as in the case of the next example where a compressible Navier–Stokes solver was used to model the flow.

It was found that activating only the number 1 and 3 actuators is enough to excite all the structural modes and, consequently, the surrounding flowfield. The reference airspeed is 80 m/s, 32% lower than the flutter speed of 117 m/s. All the time histories were obtained for 1000 time steps with $\Delta t \equiv \Delta x / V_{\text{ref}} = 1.19e^{-4}$. The SCI/ERA algorithm [13] was used for system identification. The sizes of the aeroelastic ROMs produced are 112 (na = 0), 193 (na = 12), and 195 (na = 60).

Figure 5 shows eigenvalues of the identified aerodynamic system with na = 60 in the discrete-time domain. The size of the aerodynamic matrix is (171 × 171), and all the eigenvalues are seen to be stable; that is, they are within the unit circle of the Z domain. Figure 6 is the aeroelastic root locus plot for the three identified ROMs vs the full-order model (FOM) at the reference speed. Note that only the circulatory terms were accounted for in these calculations. It can be seen that all four sets of roots match extremely well. Figure 7 is another comparison at the flutter speed, $V = 117$ m/s. For this calculation, the structural model was discretized again with a new time step, $\Delta t \equiv \Delta x / V = 8.14e^{-5}$ From Figs. 6 and 7, it can be concluded that when sufficient aerodynamic samples are available (e.g., na = 60), the eigenvalues of the ROM match very well with those of the FOM for a wide range of airspeeds, a point which will be made more clear in the next example. Note that even if there are not

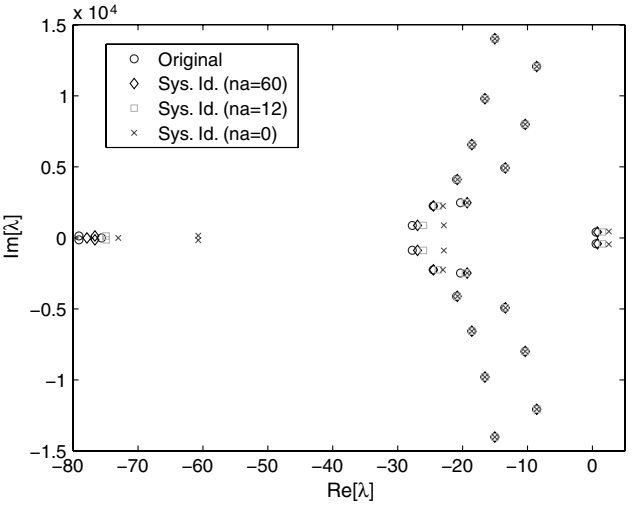

Fig. 7 Aeroelastic roots of VLM wing (circulatory part only) at $V = 117$ m/s.

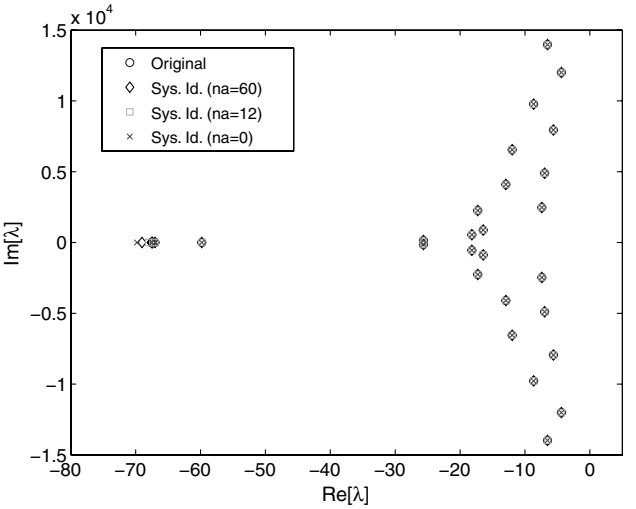

Fig. 8 Aeroelastic roots of VLM wing (noncirculatory and circulatory parts) at $V_{\text{ref}} = 80$ m/s.

[†]Information received from presentation on computational methods on aeroelasticity by G. Sengupta, T. Kim, and J. Castro at the 48th AIAA/ASME/ASCE/AHS/ASC Structures, Structural Dynamics, and Materials Conference in April 2007.

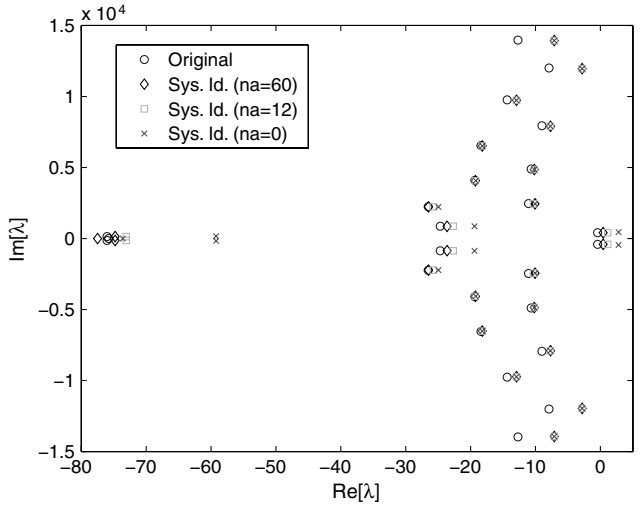

Fig. 9 Aeroelastic roots of VLM wing (noncirculatory and circulatory parts) at $V = 117$ m/s.

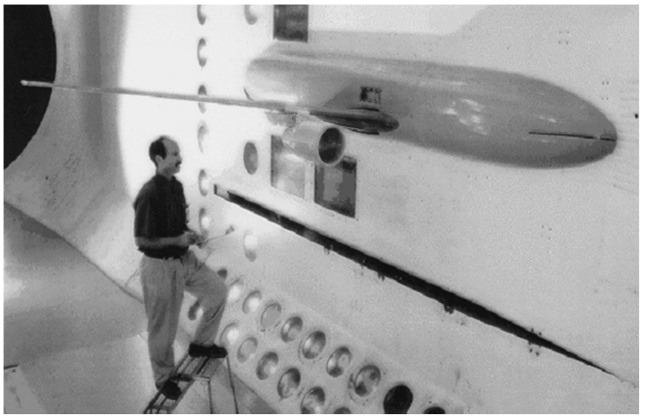

Fig. 10 TETFM in the transonic dynamic tunnel.

enough aerodynamic data, the ROM results still compare fairly well, although one can expect they will eventually fall apart as the reference point gets further away from the flutter point. The result from the case with zero aerodynamic data is especially encouraging because, in many ways, this scenario closely resembles the actual FFT in which, for practical reasons, unsteady pressure gauges may not be readily available. In particular, Fig. 7 shows that with structural samples alone, the method can predict the onset of flutter fairly accurately, provided that the reference speed is not too far from the flutter point. Mathematically, without the aerodynamic samples, the aeroelastic system is not fully realizable due to the rank deficiency in the data set. Nevertheless, it can be speculated that, since a certain amount of the aerodynamic information is embedded in the aeroelastic states, the aerodynamics identified herein would match well with the original system in the neighborhood of the reference condition. Figures 8 and 9 show aeroelastic roots with both the noncirculatory and circulatory terms in the aerodynamics. As expected, the eigenvalues predicted by the ROMs are less accurate in the high-frequency region due to the presence of the noncirculatory aerodynamics that do not comply with the format of the aerodynamic equation of motion used in the current ROMs.

Twin-Engine Transport Flutter Wind-Tunnel Model in Transonic Viscous Flow

The next example is a representative Boeing commercial model that was tested in a transonic wind tunnel, also known as the twin-engine transport flutter model (TETFM) (Fig. 10). Its aeroelastic modeling and behavior were thoroughly investigated in the past [10]. The reference flow condition is summarized as follows: the fluid is Freon with a purity of 0.8, the Mach number is 0.831, the angle of attack is 2.05 deg, q is 149 psf (1.035 psi), and the Re is 2,700,000.

In addition to the wing motion described by the 10 mode shapes (Fig. 11), 10 GAFs were recorded during numerical simulations. The natural frequencies of the first four modes are 7.53, 14.63, 17.69, and 22.92 Hz, respectively. Time histories of these responses were obtained by coupling (10×10) generalized aerodynamic impulse functions with the generalized structural coordinates and integrating them in the time domain. The aerodynamic impulse functions were generated previously by applying an impulse in each of the 10 generalized coordinates with 0.001 magnitude of amplitude [10]. Although indirect, when convoluted with the structural states, this approach produces the same results as the fully coupled fluid–structure equations. It is much more convenient and faster to change the dynamic pressure using the coupled solution technique; therefore, it is suitable for the current study. To examine the effect of aerodynamic measurement, the system identification was also performed with 0, 30, and 160 aerodynamic samples. They are artificial pressure data obtained based on the state-space aerodynamic ROM available from the previous reference. More specifically, arbitrary linear combinations of the state variables that define the state-space aerodynamic model were taken and used as the aerodynamic samples. These aerodynamic states do not represent the physical pressures but are related to the physical pressures through the linear state-space equations. Once again, since the structural model was already known from the ELFINI program, no separate system identifications were necessary for the structure and the (10×10) generalized mass, stiffness matrices were used to construct (20×20) the structural system. Thus, the total number of aeroelastic measurements available was 20 (na $= 0$), 30 (na $= 10$), 50 (na $= 30$), and 180 (na $= 160$). Since the wing model does not have control surfaces, it was necessary to make up control inputs for the numerical simulations. For this purpose, the two inputs used for the previous rectangular wing were borrowed. While this type of actuation is by no means realistic, it nevertheless serves as a valid way to excite the wing structure and, subsequently, the unsteady flowfield. Alternatively, if the computational model does not have the option of adding control inputs, one can run the simulation with an initial condition, for it would be mathematically equivalent to using a

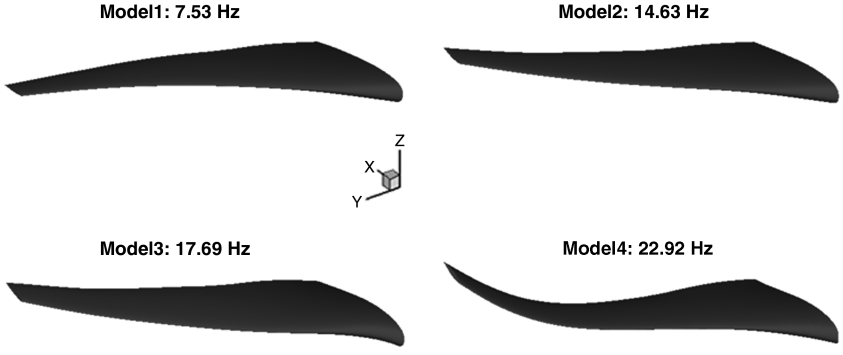

Fig. 11 First four structural modes of TETFM model.

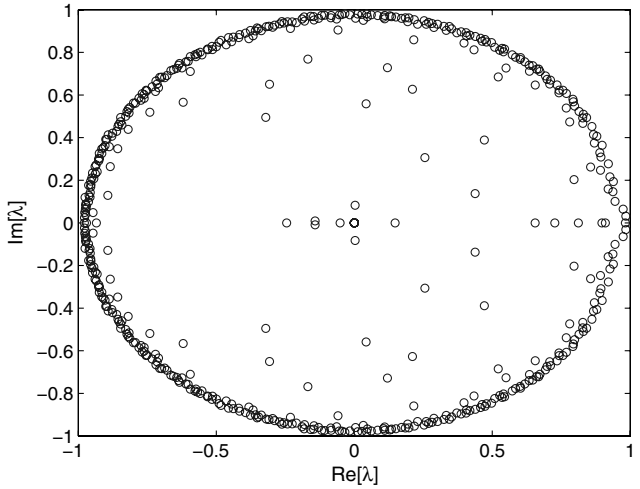

Fig. 12 Aerodynamic eigenvalues of TETFM model in the discrete-time domain (WT denotes wind tunnel).

control vector with an impulse time function. The coupled ELFINI/CFL3D aeroelastic solutions were obtained by time marching for 995 steps with the incremental time step, $\Delta t = 3.34\text{e} - 004$ s, at the reference dynamic pressure $q_{\text{ref}} = 1.035$ psi, subject to the two impulse inputs. As before, the SCI/ERA algorithm was used for the system identification. The sizes of the aeroelastic ROMs produced are 476(na = 0), 350(na = 10), 519(na = 30), and 538(na = 160).

Figure 12 shows eigenvalues of the identified aerodynamic system with na = 160. Once again, all the eigenvalues are stable, staying within the unit circle of the Z domain. Figures 13–18 show comparisons of diagonal and offdiagonal elements of the GAF

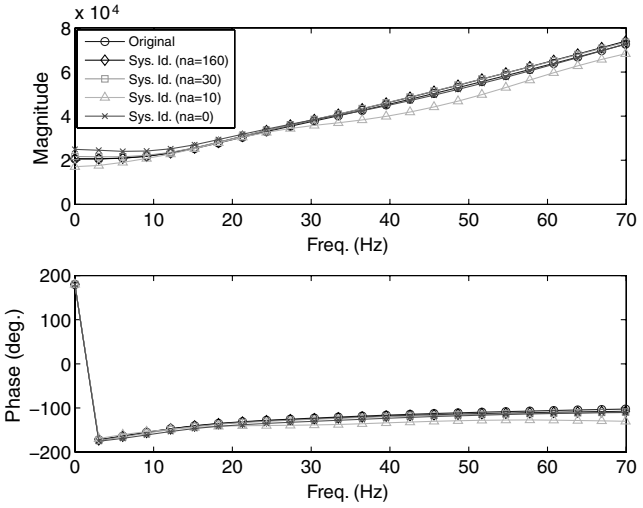

Fig. 13 TETFM model GAF Q_{11}.

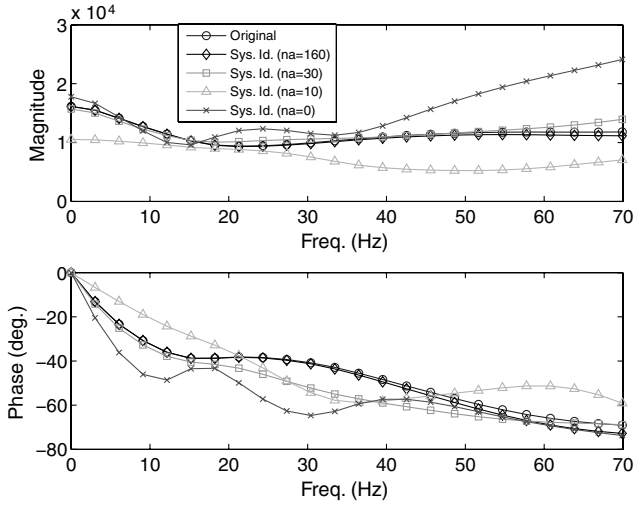

Fig. 14 TETFM model GAF Q_{33}.

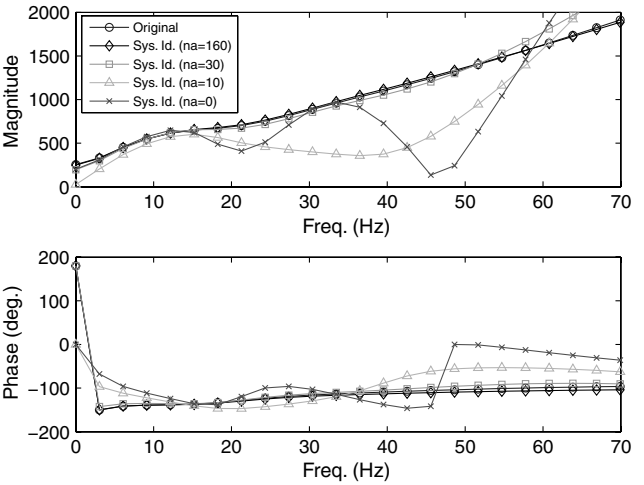

Fig. 15 TETFM model GAF Q_{22}.

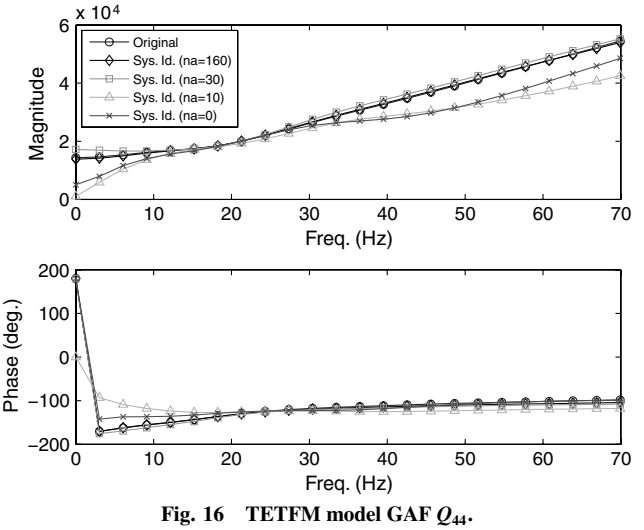

Fig. 16 TETFM model GAF Q_{44}.

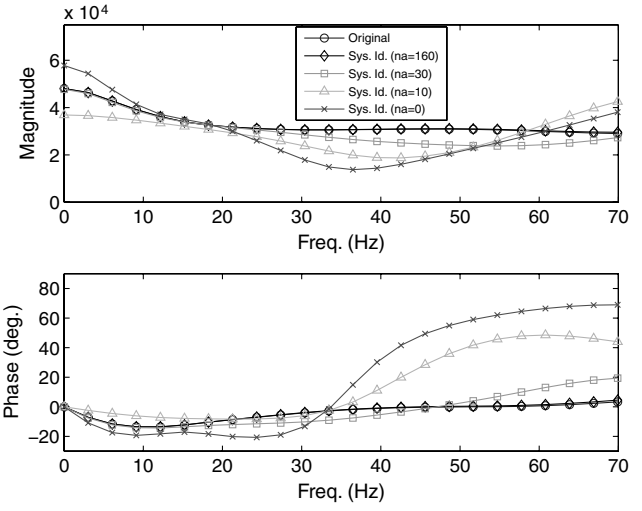

Fig. 17 TETFM model GAF Q_{13}.

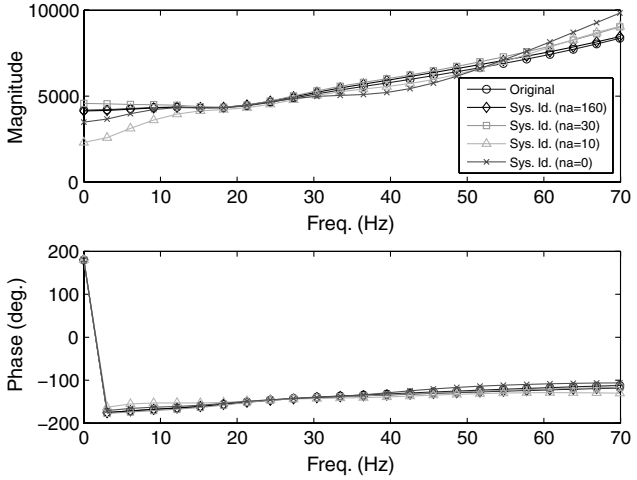

Fig. 18 TETFM model GAF Q_{24}.

matrix between the original CFL3D model and the identified aerodynamic models. It can be seen that when a sufficient number of aerodynamic samples are available (na = 160), the new method reproduces the aerodynamic forces extremely accurately for the entire frequency range of interest. In fact, even with na = 80, all the results seem to converge well. The results also show that, even without aerodynamic data (na = 0), the GAFs match well in the vicinity of the natural frequencies of the mode shapes. Just how much and when the identified aerodynamic model will differ from the CFD depends on the type of mode shape and the location of the frequency. For instance, the method with zero aerodynamic samples seems to reproduce Q_{11}, a component responsible for both the first and second flutters, very well for a very wide range of frequencies. Note the simple shape of this mode, which mainly consists of the first wing bending (Fig. 11). On the other hand, for higher modes where the mode shapes are more complicated, its results are not very accurate, except near the frequencies at which the mode shapes oscillate in the aeroelastic simulations. Note that these frequencies would be close to the natural frequencies of the mode shapes, especially at a low dynamic pressure.

Figures 19 and 20 are Vg plots for all 10 modes of the three cases of na = 0, 10, and 160. These results were obtained by varying the dynamic pressure while keeping the incremental time at the constant value. For the clarity of the figures, results from the case with na = 30 are not included, but it is reported that they fall somewhere between those of na = 10 and na = 160. As expected, when na = 160, the correlation between the FOM and the ROM is excellent. It must be noted that adding the 10 GAF samples produces accurate aeroelastic

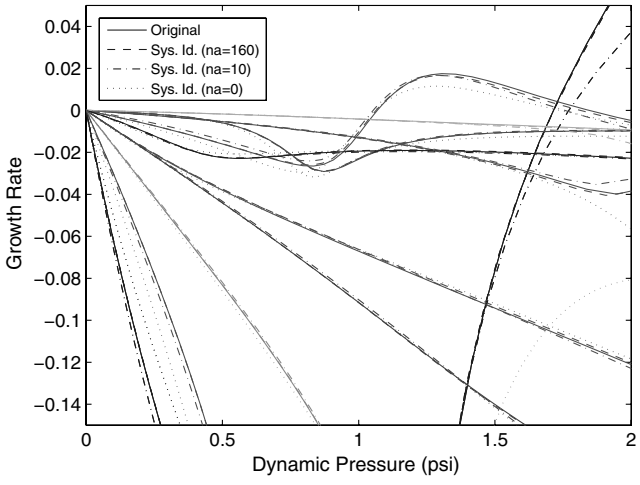

Fig. 19 TETFM model damping vs dynamic pressure: q_{ref}= 1.035 psi.

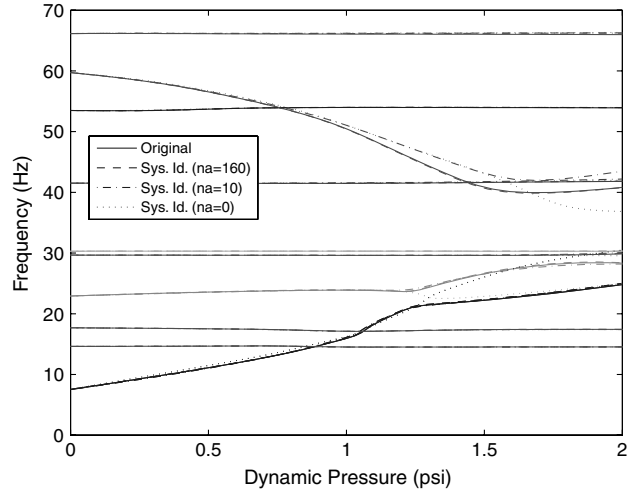

Fig. 20 TETFM model frequency vs dynamic pressure: q_{ref}= 1.035 psi.

damping and frequency results, capturing both the first and second flutter points at $q = 1.069$ psi and $q = 1.715$ psi with a surprisingly good accuracy, with less than 3 and 4% errors, respectively. The identified model using the structural response samples alone also predicts the first flutter fairly well, with a less than 1% error, but it misses the second instability completely. The frequencies, on the other hand, are better predicted for all of the modes when the

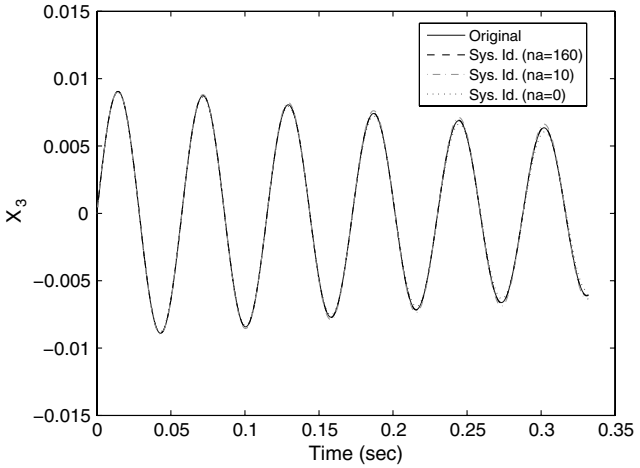

Fig. 21 TETFM model aeroelastic response at $q = 0.75$ psi.

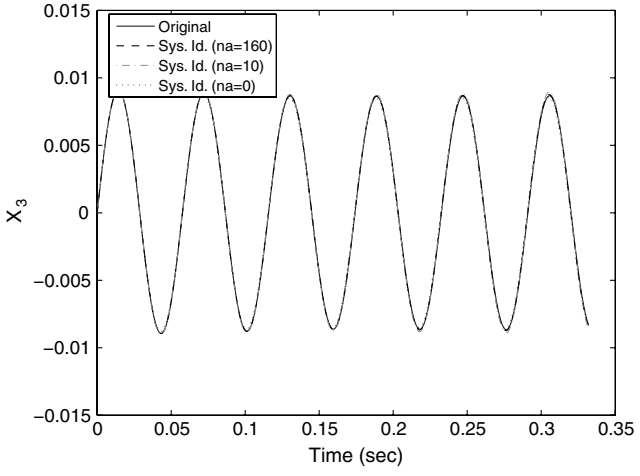

Fig. 22 TETFM model aeroelastic response at $q = 1.069$ psi.

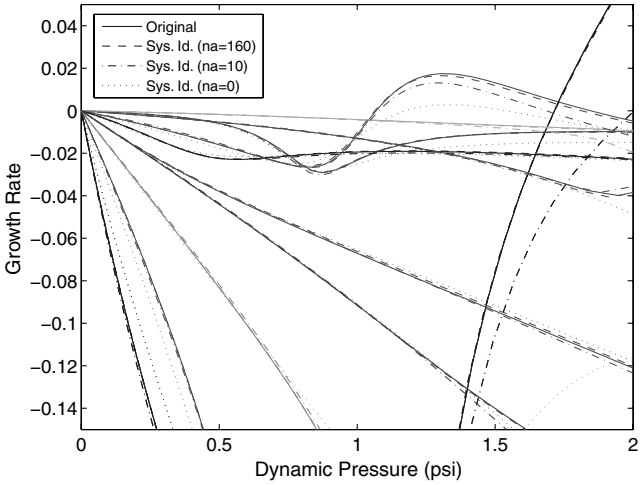

Fig. 23 TETFM model damping vs dynamic pressure: $q_{\text{ref}} = 0.75$ psi.

aerodynamic samples are included in the system identification. Figures 21 and 22 are time histories at the subcritical ($q = 0.75$ psi) and first flutter ($q = 1.069$ psi) points, showing a good match between the FOM and the ROMs.

Figures 23 and 24 are the Vg plots again, except that the new ROMs were constructed at $q = 0.75$ psi, 32% lower than the first flutter point. The sizes of the resulting aeroelastic ROMs are 473 (na = 0), 350 (na = 10), and 538 (na = 160). Once again, with na = 160, the method generates extremely accurate modal damping and frequency results for the entire range of dynamic pressure covered, clearly suggesting that, as long as enough aerodynamic samples are used, the aerodynamic ROM can reproduce all the GAFs accurately, regardless of its reference dynamic pressure. Otherwise, since the new reference point is further away from the instability point, the new ROMs do not predict nearly as well as the previous ROMs. It is still encouraging that, with just the 10 GAF data, it once again predicts the first flutter very well, with less than 1% error, although the prediction gets off by 9.9% with no aerodynamic data. In particular, the present method can reproduce the highly nonlinear curve in the damping of critical mode 3 that starts around $q = 0.7$ psi and continues up to the upper bound of $q = 2$ psi.

Finally, a comment on CPU time to generate the aeroelastic ROMs is in order. In [10], it was reported that a typical CPU time for generating the (10×10) aerodynamic impulse responses was 366 h. Considering that running the coupled ELFINI/CFL3D aeroelastic solver would not take much longer than solving the CFL3D code and only two inputs were used in all of the aeroelastic simulations, the overall CPU time would be close to $\frac{366}{5} = 73.2$ h, yielding a saving factor of five. This CPU time could be further reduced by using a simultaneous excitation of the two inputs, e.g., using the SCI/ERA or OKID method.

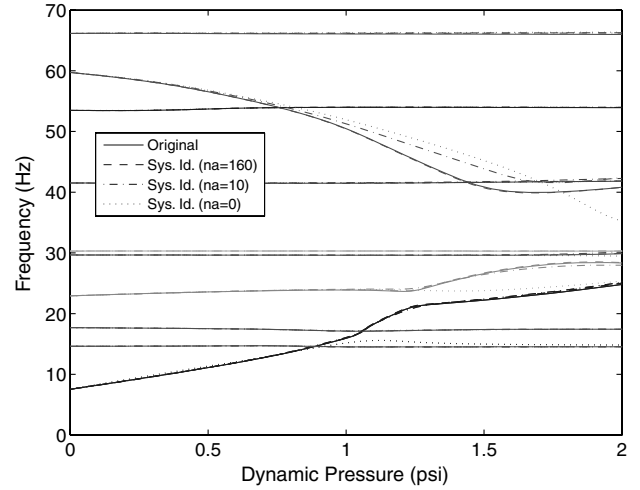

Fig. 24 TETFM model frequency vs dynamic pressure $q_{\text{ref}} = 0.75$ psi.

Conclusions

The following statements are the summary of the new system identification and model reduction method for the coupled fluid–structure system: aerodynamics is aeroelasticity minus structure (AAEMS):

1) Using transformations between structural and aeroelastic states, we have derived an unsteady aerodynamic system equation by subtracting the structural states from the aeroelastic states.

2) The GAFs identified herein are valid for all frequency ranges, provided that the aeroelastic system realized by $(\mathbf{A}_t, \mathbf{B}_t, \mathbf{C}_t)$ is aerodynamically rich. To generate such a system, one must take sufficient aerodynamic measurements such that the sampled data are fully ranked. Otherwise, the GAFs produced will only be accurate in the neighborhood of oscillation frequencies of the structural modes.

3) Samples of the structural response alone can predict the onset of the first flutter fairly well, provided they are not taken too far from the critical point. This simple technique could be easily employed for aeroelastic damping and flutter prediction based on FFT data.

4) The identification procedure is fast and straightforward; hence, it is suitable for a variety of aeroelastic analyses, including flutter prediction, dynamic loads calculation, optimization, and closed-loop controller design.

The method needs to be validated for realistic configurations with added samples of local pressure measurements. More research needs to be done to investigate the effects of control inputs and the locations of structural responses and to find optimal locations of the pressure samples.

The following are anticipated applications and advantages of AAEMS when applied to CSD/CFD:

1) It is possible to construct an aeroelastic ROM using aeroelastic responses sampled at a single dynamic pressure subject to a few excitation inputs. There is no need to do the multiple mode-by-mode GAFs calculations. Considering that running the coupled aeroelastic solver does not take much longer than solving the CFD code, the overall savings in CPU time will be quite significant.

2) The necessity of dealing with CFD directly is minimized, as the method requires time history samples for only structure and aeroelasticity. This is a big advantage for structural engineers who are not familiar with the CFD code.

When applied to WTT and FFT, the following advantages are anticipated:

1) For a fixed Mach condition, it is feasible to get the damping, the frequency, and the mode shape of the critical modes for all speeds by using data obtained at a single subcritical condition.

2) It is feasible to predict the onset of flutter using the data taken at the single flight condition.

3) It is feasible to experimentally (but indirectly) identify the GAF matrix for flexible mode shapes and adjust or replace the unsteady aerodynamic forces in the current low-order analytical models (e.g., doublet lattice).

As a final note, [20] represents the first work in which the system identification was applied to experimental data obtained from a WTT.

Acknowledgment

The author is grateful to Frank T. Roney for his continuous support during this research.

References

[1] Hall, K. C., "Eigenanalysis of Unsteady Flows About Airfoils, Cascades, and Wings," *AIAA Journal*, Vol. 32, No. 12, 1994, pp. 2426–2432.
doi:10.2514/3.12309

[2] Dowell, E. H., Hall, K. C., and Romanowski, M. C., "Eigenmode Analysis in Unsteady Aerodynamics, Reduced-Order Models," *Applied Mechanics Reviews*, Vol. 50, No. 6, 1997, pp. 371–386.

doi:10.1115/1.3101718
[3] Romanowski, M. C., "Reduced-Order Unsteady Aerodynamic and Aeroelastic Models Using Karhunen–Loeve Eigenmodes," AIAA Symposium on Multidisciplinary Analysis and Optimization, Bellevue, WA, AIAA Paper 1996-3981, 1996.
[4] Kim, T., "Frequency-Domain Karhunen-Loeve Method and Its Application to Linear Dynamic Systems," *AIAA Journal*, Vol. 36, No. 11, 1998, pp. 2117–2123. doi:10.2514/2.315
[5] Hall, K., Thomas, J. P., and Dowell, E., "Proper Orthogonal Decomposition Technique for Transonic Unsteady Aerodynamic Flows," *AIAA Journal*, Vol. 38, No. 10, 2000, pp. 1853–1862. doi:10.2514/2.867
[6] Kim, T., and Bussoletti, J. E., "An Optimal Reduced-Order Aeroelastic Modeling Based on a Response-Based Modal Analysis of Unsteady CFD Models," 42nd AIAA/ASME/ASCE/AHS/ASC Structures, Structural Dynamics, and Materials Conference, Seattle, WA, AIAA Paper 2001-1525, April 2001.
[7] Silva, W. A., "Application of Nonlinear Systems Theory to Transonic Unsteady Aerodynamic Responses," *Journal of Aircraft*, Vol. 30, No. 5, 1993, pp. 660–668. doi:10.2514/3.46395
[8] Silva, W. A., and Bartels, R. E., "Development of Reduced-Order Models for Aeroelastic Analysis and Flutter Prediction Using the CFL3Dv6.0 CFD Code," *Journal of Fluids and Structures*, Vol. 19, No. 6, 2004, pp. 729–745. doi:10.1016/j.jfluidstructs.2004.03.004
[9] Raveh, D. E., "Identification of Computational Fluid Dynamic Based Unsteady Aerodynamic Models for Aeroelastic Analysis," *Journal of Aircraft*, Vol. 41, No. 3, 2004, pp. 620–632. doi:10.2514/1.3149
[10] Kim, T., Hong, M., Bhatia, K. G., and Sengupta, G., "Aeroelastic Model Reduction for Affordable Computational Fluid Dynamics-Based Flutter Analysis," *AIAA Journal*, Vol. 43, No. 12, 2005, pp. 2487–2495. doi:10.2514/1.11246
[11] Gupta, K. K., and Bach, C., "Systems Identification Approach for a Computational-Fluid-Dynamics Based Aeroelastic Analysis," *AIAA Journal*, Vol. 45, No. 12, 2007, pp. 2820–2827. doi:10.2514/1.28647
[12] Schuster, D. M., Liu, D. D., and Huttsell, L. J., "Computational Aeroelasticity: Success, Progress, Challenge," *Journal of Aircraft*, Vol. 40, No. 5, 2003, pp. 843–856. doi:10.2514/2.6875
[13] Kim, T., "Efficient Reduced-Order System Identification for Linear Systems with Multiple Inputs," *AIAA Journal*, Vol. 43, No. 7, 2005, pp. 1455–1464. doi:10.2514/1.11225
[14] Silva, W., "Simultaneous Excitation of Multiple-Input/Multiple-Output CFD-Based Unsteady Aerodynamic Systems," *Journal of Aircraft*, Vol. 45, No. 4, 2008, pp. 1267–1274. doi:10.2514/1.34328
[15] Amsallem, D., and Farhat, C., "Interpolation Method for Adapting Reduced-Order Models and Application to Aeroelasticity," *AIAA Journal*, Vol. 46, No. 7, 2008, pp. 1803–1813. doi:10.2514/1.35374
[16] Nissim, E., and Gilyard, G. B., "Method for Experimental Determination of Flutter Speed by Parameter Identification," NASA TP 2923, 1989.
[17] Juang, J.-N., *Applied System Identification*, Prentice–Hall, Englewood Cliffs, NJ, 1994.
[18] Box, G., Jenkins, G. M., and Reinsel, G. C., *Time Series Analysis: Forecasting and Control*, 3rd ed., Prentice–Hall, Englewood Cliffs, NJ, 1994.
[19] Bisplinghoff, R. L., Ashley, H., and Halfman, R. L., *Aeroelasticity*, Dover, Mineola, NY, 1983.
[20] Song, J., Song, S. J., and Kim, T., "Experimental Determination of Unsteady Aerodynamic Coefficients and Flutter Behavior of a Rigid Wing," 51st AIAA/ASME/ASCE/AHS/ASC Structures, Structural Dynamics, and Materials Conference, Orlando, FL, AIAA Paper 2010-2875, April 2010.

P. Beran
Associate Editor